

# Unifying autocatalytic and zeroth order branching models for growing actin networks

Julian Weichsel,<sup>1,2,\*</sup> Krzysztof Baczynski,<sup>1</sup> and Ulrich S. Schwarz<sup>1,†</sup>

<sup>1</sup>*Bioquant and Institute for Theoretical Physics, University of Heidelberg, Germany*

<sup>2</sup>*Department of Chemistry, University of California at Berkeley, United States*

(Dated: July 20, 2012)

The directed polymerization of dendritic actin networks is an essential element of many biological processes, including cell migration. Different theoretical models for the interplay between the underlying processes of polymerization, capping and branching have resulted in conflicting predictions. One of the main reasons for this discrepancy is the assumption of a branching reaction which is first (autocatalytic) versus zeroth order in filament density. Here we introduce a unifying framework from which these two models emerge as limiting cases for low and high filament density, respectively. A smooth transition between these cases is found at intermediate conditions. We also derive a threshold for the capping rate, below which zeroth order characteristics are predicted to dominate the dynamics of the network for all accessible filament densities. For capping rates above this threshold, autocatalytic growth is predicted at sufficiently low filament density.

In many situations of high biological relevance, including the migration of animal cells and the movement of intracellular pathogens such as the bacterium *Listeria*, motility and force generation results from the directed polymerization of a dendritic actin filament network [1]. The organization of the growing network is determined mainly at the leading edge, where a small number of proteins regulates the interplay between three fundamental processes. The driving force for propulsion is polymerization of actin filaments from globular actin monomers, which is directly counterbalanced by filament capping through specialized capping proteins. In addition, daughter filaments are branched off from mother filaments [2]. Although the biochemical details of this process are not completely understood, it is widely accepted that the branching complex Arp2/3 is activated by nucleation promoting factors (NPFs). When an activated Arp2/3-complex is bound to the side of an existing actin filament, a daughter filament starts to grow at a characteristic angle around  $70^\circ$  relative to the mother filament (compare Fig. 1a). The interplay between the three fundamental processes of polymerization, capping and branching is force-dependent and leads to a non-trivial force-velocity relation that is essential for understanding e.g. cell motility.

Due to the high biological relevance and universal nature of the underlying processes, many theoretical models have been suggested to describe the characteristic features of growing actin networks [3]. However, in many cases contradictory predictions have been obtained, in particular regarding the force-velocity relation [4–10] and the spatial organization of the network [11–14]. Interestingly, many of these contradictions are a direct consequence of two different choices for the order of the branching reaction. In *autocatalytic models*, the total rate of

branching is assumed to be proportional to the number of existing filaments in the network, i.e. it is modeled as a *first order* reaction in filament density, implicitly assuming an unlimited reservoir of activated Arp2/3 [11, 15, 16]. This yields growing actin networks for which a constant filament density is maintained only at a unique steady state growth velocity. Increasing forces acting against the network reduce the speed of growth only transiently, as an increasing filament density subsequently lowers the force per filament back to the stationary level.

In marked contrast to the autocatalytic models, another class of models assumes that branching occurs with a constant rate, i.e. it is taken to be a *zeroth order* reaction in filament density, corresponding to a limited supply of activated Arp2/3 [12, 15, 17]. Under these conditions, it has been shown that a continuum of steady state velocities exists. Moreover two competing steady state filament orientation patterns are stable, namely the  $\pm 35^\circ$  and  $+70/0/-70^\circ$  patterns shown schematically in Fig. 1b and c, respectively. Transitions between these two fundamentally different network architectures can be triggered by changes in network growth velocity [17]. Indeed similar structural transitions have been demonstrated recently with electron microscopy for the lamellipodium of keratocytes [13, 14]. In this Letter, we will show that the two contradictory model scenarios of autocatalytic and

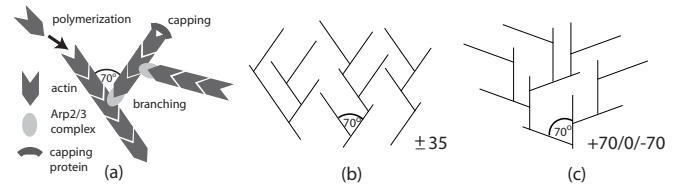


FIG. 1: (a) Interplay of polymerization, capping and branching at the leading edge of an actin network growing towards the top. (b) A  $\pm 35^\circ$  pattern is usually associated with dendritic actin networks. (c) However, for certain parameter values a  $+70/0/-70^\circ$  pattern can become stable.

\*Electronic address: weichsel@berkeley.edu

†Electronic address: ulrich.schwarz@bioquant.uni-heidelberg.de

zeroth order branching can be unified within a general theoretical framework that reconciles some of the seemingly contradictory observations and predictions.

*Model definition.* Because the lamellipodium of cells migrating on flat substrates is very thin, we consider a two-dimensional model for a growing actin network. Following earlier work along these lines [11, 15, 17], we consider the distribution function  $N(\theta, t)$  for the number of uncapped filaments per area orientated at time  $t$  at the angle  $\theta$  with regard to the normal of the leading edge. We assume  $N(\theta, t)$  to be defined in a small reaction region of width  $d_{br}$  behind the leading edge, in which Arp2/3 activation by NPFs and subsequent branching of new filaments is possible. Its time evolution is described by the kinetic equation

$$\frac{dN(\theta, t)}{dt} = k_b \frac{\int_{-\pi}^{+\pi} \mathcal{W}(\theta, \theta') N(\theta', t) d\theta'}{\left( \int_{-\pi}^{+\pi} \int_{-\pi}^{+\pi} \mathcal{W}(\theta, \theta') N(\theta', t) d\theta' d\theta \right)^{1-\mu}} - k_c N(\theta, t) - k_{gr}^\theta(v_{nw}) N(\theta, t), \quad (1)$$

where the three terms on the right hand side describe the effects of branching, capping and outgrowth from the reaction region, respectively. While capping is assumed to be a first order reaction in  $N$  with rate  $k_c$ , the order of the branching reaction is assumed to be variable and described by the dimensionless parameter  $\mu$ . The two cases  $\mu = 0$  and  $\mu = 1$  correspond to zeroth and first order branching, respectively. Values of  $0 < \mu < 1$  interpolate between these two cases.  $k_b$  is the rate of branching and  $\mathcal{W}(\theta, \theta') = \mathcal{W}(|\theta - \theta'|)$  is the distribution function for the orientation  $\theta$  of a daughter filament branching off from a mother filament with orientation  $\theta'$ . Motivated by experimental observations, we approximate this function by the renormalized sum of two Gaussians centered around  $\pm 70^\circ$  and each with standard deviation  $5^\circ$  (the detailed values are not relevant for our results). The third term in Eq. (1) describes the rate at which filaments are growing out of the reaction region. We assume a well-defined network growth velocity  $v_{nw}$ , which has to be compared with the single filament polymerization velocity  $v_{fil}$ . For  $|\theta| \leq \arccos(v_{nw}/v_{fil})$ , the single filaments can keep up with the leading edge and we have  $k_{gr}^\theta(v_{nw}) = 0$ . If the orientation angle exceeds the threshold, however, the single filaments grow too slowly and leave the reaction region with a rate  $k_{gr}^\theta(v_{nw}) = (v_{nw} - v_{fil} \cos \theta)/d_{br}$ .

Our model has only four relevant parameters, the rates  $k_c$  and  $k_b$  for capping and branching, respectively, the network growth velocity  $v_{nw}$  and the order  $\mu$  of the branching reaction. We solve it numerically by discretizing Eq. (1) in 360 values for  $\theta$ . In the following, we compare these results to two other versions of the model [17]. In a more detailed model, which does not use the distribution function  $N(\theta, t)$ , we perform stochastic computer simulations of individual filaments evolving according to the rules described above. In a simplified analytical version of the reaction model Eq. (1), we integrate over  $35^\circ$  sized angle bins and neglect contributions of filaments

with growth directions  $> 87.5^\circ$ . This leads to a set of three coupled equations:

$$\begin{aligned} \frac{dN_{0^\circ}}{dt} &= \frac{1}{2} k_b \frac{N_{\pm 70^\circ}}{\left( \sum_i N_i \right)^{(1-\mu)}} - k_c N_{0^\circ} \\ \frac{dN_{\pm 35^\circ}}{dt} &= \frac{1}{2} k_b \frac{N_{\pm 35^\circ}}{\left( \sum_i N_i \right)^{(1-\mu)}} - (k_c + k_{gr}^{35^\circ}) N_{\pm 35^\circ} \\ \frac{dN_{\pm 70^\circ}}{dt} &= k_b \frac{N_{0^\circ}}{\left( \sum_i N_i \right)^{(1-\mu)}} - (k_c + k_{gr}^{70^\circ}) N_{\pm 70^\circ} \end{aligned} \quad (2)$$

where the summation is performed over the angle bins  $i = \{0^\circ, \pm 35^\circ, \pm 70^\circ\}$ .

*Steady state analysis of the analytical model.* From Eq. (2), one can show that our model has two steady state solutions,  $N^{ss70}$  and  $N^{ss35}$ :

$$\begin{aligned} N_{0^\circ}^{ss70} &= \frac{-k_c - k_{gr}^{70^\circ} + \sqrt{2k_c(k_c + k_{gr}^{70^\circ})}}{k_c - k_{gr}^{70^\circ}} \cdot A^{1/(1-\mu)} \\ N_{\pm 35^\circ}^{ss70} &= 0 \\ N_{\pm 70^\circ}^{ss70} &= \frac{2k_c - \sqrt{2k_c(k_c + k_{gr}^{70^\circ})}}{k_c - k_{gr}^{70^\circ}} \cdot A^{1/(1-\mu)} \end{aligned} \quad (3)$$

and

$$N_{0^\circ}^{ss35} = N_{\pm 70^\circ}^{ss35} = 0, \quad N_{\pm 35^\circ}^{ss35} = B^{1/(1-\mu)} \quad (4)$$

where

$$A = k_b / \sqrt{2k_c(k_c + k_{gr}^{70^\circ})}, \quad B = k_b / 2(k_c + k_{gr}^{35^\circ}). \quad (5)$$

The two fixed points of the system correspond to the two competing orientation patterns depicted schematically in Fig. 1a and b, respectively. While  $N^{ss70}$  has peaks at  $+70^\circ/-70^\circ$  degrees,  $N^{ss35}$  is peaked at  $\pm 35^\circ$  degrees.

Linear stability analysis shows that for  $\mu > 1$ , the two fixed points are both saddle points and thus no stable solutions exist. For  $\mu < 1$ , the eigenvalues for the two fixed points have opposite signs, which leads to mutual exclusive stability. Fig. 2a illustrates the regions of stability for each of the two orientation patterns within the three dimensional parameter space spanned by  $k_b$ ,  $k_c$  and  $v_{nw}$ . The two meshed surfaces represent transitions between a  $+70^\circ/-70^\circ$  pattern above and below the two surfaces and a  $\pm 35^\circ$  pattern in between. These transition surfaces are independent of  $\mu$  and  $k_b$ . Thus all cases with  $\mu < 1$  show no difference compared to a model explicitly assuming zeroth order branching [17].

The case  $\mu = 1$  (autocatalytic growth) is special and has to be discussed separately. In the limit  $\mu \rightarrow 1$ , each of the two steady state solutions can exist only if additional conditions on the parameter values are satisfied. This important aspect can be understood from Eq. (1), where for  $\mu = 1$  all three terms on the right hand side become linear in  $N$  and thus for the steady state can sum up to zero only if the three rates cancel each other. The corresponding condition is different for each of the two fixed points and can be inferred from Eq. (3) and Eq. (4), respectively, in combination with Eq. (5). For  $N^{ss70}$ , only

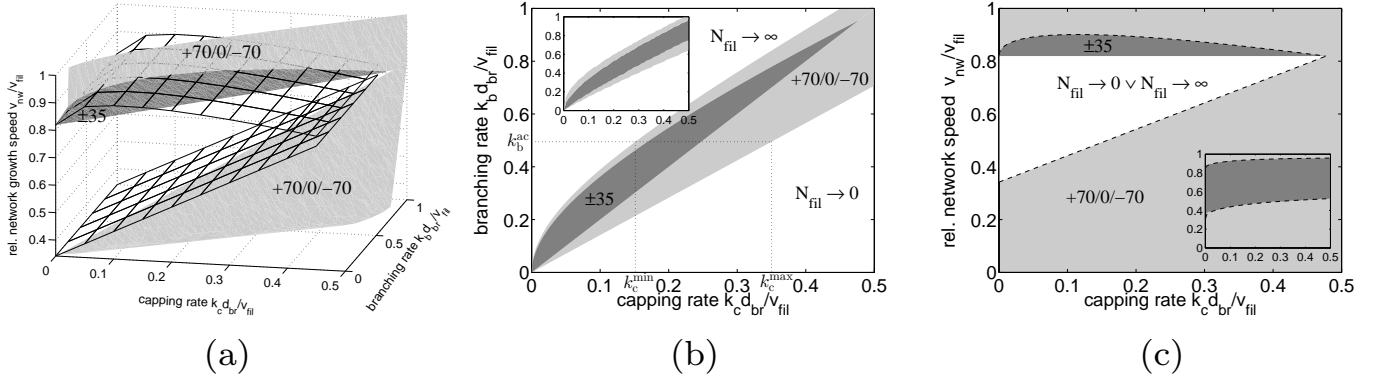


FIG. 2: Phase diagram of the analytical model. In general, two mutually exclusive stable fixed points exist, the  $\pm 35$  and  $+70/0/-70$  patterns shown in Fig. 1a and b. (a) For  $\mu < 1$  the parameter space is three-dimensional, with the  $\pm 35$  pattern being stable between the two meshed surfaces. The  $+70/0/-70$  pattern is stable above and below these two surfaces. For the case  $\mu = 1$  (autocatalytic growth), only one network growth velocity is possible and the stable solutions are restricted to the dark and light gray surfaces for the  $\pm 35$  and  $+70/0/-70$  patterns, respectively. The simplifications of the analytic model lead to a jump discontinuity at the lower transition. (b) Autocatalytic model ( $\mu = 1$ ) in the  $k_c$ - $k_b$  plane. Here the jump discontinuity is not visible. The inset demonstrates the good agreement between the analytical and the full numerical solutions.  $k_c^{\min}$  and  $k_c^{\max}$  show the parameter region over which autocatalytic growth is possible for the given effective branching rate  $k_b^{\text{ac}}$  (see Eq. (10) and Eq. (11) below). (c) Autocatalytic model in the  $k_c$ - $v_{\text{nw}}$  plane. Here the jump discontinuity leads to a region where no velocity with finite  $N$  exists. The result from the full numerical solution (inset) does not share this property.

$A = 1$  gives a finite solution for  $\mu \rightarrow 1$ , thus we require  $k_{\text{gr}}^{70^\circ}(v_{\text{nw}})k_c + k_c^2 = k_b^2/2$ . For  $N^{\text{ss}35}$ , only  $B = 1$  gives a finite solution for  $\mu \rightarrow 1$ , thus we require  $k_{\text{gr}}^{35^\circ}(v_{\text{nw}}) + k_c = k_b/2$ . We conclude that for  $\mu = 1$ , a finite filament density in steady state is only observed at one unique network velocity for each combination of  $k_b$  and  $k_c$ , as is expected for autocatalytic growth [15].

In Fig. 2a, the two conditions resulting from  $A = 1$  and  $B = 1$  are shown as light and dark gray surfaces, respectively. Because the simplified model is too restricting as to be able to realize any value for network growth velocity, there is a jump discontinuity to the lower transition (at the upper transition, the two surfaces coincide). In Fig. 2b and c, we show the projections of the phase diagram for  $\mu = 1$  from Fig. 2a onto the  $k_c$ - $k_b$  and  $k_c$ - $v_{\text{nw}}$  planes, respectively. In Fig. 2b, the jump discontinuity is not visible. In Fig. 2c, it leads to a region with velocity values that do not yield finite  $N_{\text{fil}}$ . Note however that this special property only occurs as an artefact of the simplifications made for analytical progress. The insets in Fig. 2b and c show the phase diagrams obtained from the full numerical analysis of Eq. (1). In contrast to the analytical model, they show no jump discontinuity and a larger stability region of the  $\pm 35$  pattern at high capping rates. Otherwise the agreement is very good, demonstrating the strength of the analytical results.

*Reaction model for branching.* Until now we have treated the order  $\mu$  of the branching reaction as a phenomenological constant. In order to relate  $\mu$  to filament density, we now introduce a reaction model for branching, based on a likely scenario for the involved biochemical steps [18, 19]. We consider two variables: Arp is the concentration of Arp2/3 that is bound to the filaments,

but did not lead to a daughter branch yet. Npf is a fraction of the total concentration of obstacle bound NPFs at the leading edge ( $\text{Npf}_0$ ) which are available to activate bound Arp2/3 complexes to nucleate a daughter branch. The kinetic equations are

$$\begin{aligned} \frac{d\text{Arp}}{dt} &= k_+ N_{\text{fil}} - \left(k_- + \frac{v_{\text{nw}}}{d_{\text{br}}}\right) \text{Arp} - \tilde{k}_b \text{Arp} \text{Npf}, \\ \frac{d\text{Npf}}{dt} &= -\tilde{k}_b \text{Arp} \text{Npf} + k_{\text{act}} (\text{Npf}_0 - \text{Npf}). \end{aligned} \quad (6)$$

Arp increases as more complexes bind to the filaments with rate  $k_+$ . It decreases due to dissociation (rate  $k_-$ ), outgrowth (rate  $v_{\text{nw}}/d_{\text{br}}$ ) and activation (rate  $\tilde{k}_b$ ). This activation step also decreases Npf as we assume NPFs that activate Arp2/3 to be occupied for additional interactions with other Arp2/3 complexes until they become available again at rate  $k_{\text{act}}$ .

In steady state, the effective rate of branching is

$$\text{BR}^{\text{ss}}(N_{\text{fil}}) = \tilde{k}_b \text{Arp}_{\text{ss}} \text{Npf}_{\text{ss}}, \quad (7)$$

which is shown in Fig. 3 for a typical set of parameters. At low filament number, we can expand the right hand side of Eq. (7) to linear order in  $N_{\text{fil}}$ :

$$\text{BR}_0^{\text{ss}} = \frac{\text{Npf}_0 d_{\text{br}} k_+ \tilde{k}_b}{\text{Npf}_0 d_{\text{br}} \tilde{k}_b + d_{\text{br}} k_- + v_{\text{nw}}} N_{\text{fil}} = k_b^{\text{ac}} N_{\text{fil}} \quad (8)$$

thus defining an autocatalytic rate  $k_b^{\text{ac}}$ . In the limit of large filament density,  $\text{BR}^{\text{ss}}$  approaches a constant:

$$\text{BR}_\infty^{\text{ss}} = \text{Npf}_0 k_{\text{act}} \quad (9)$$

and hence a zeroth order branching rate. Thus the cases of autocatalytic growth ( $\mu = 1$ ) and zeroth order branching ( $\mu = 0$ ) emerge as the limits for low and high filament

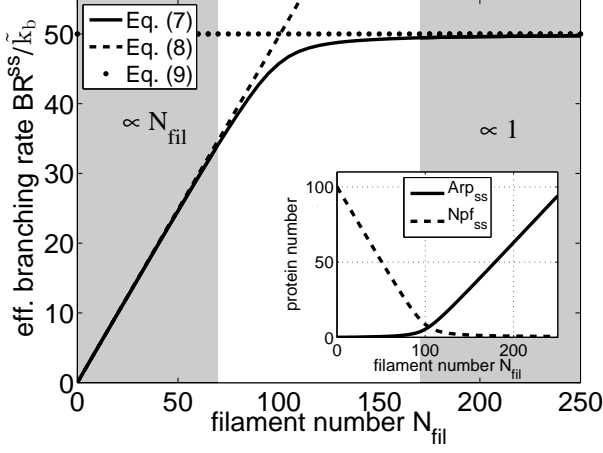


FIG. 3: Effective branching rate  $BR^{ss}$  as a function of the number of filaments  $N_{fil}$  in steady state growth. For low filament number the branching reaction is linear (autocatalytic) as given in Eq. (8) (dashed line), while in the limit of high filament number zeroth order branching is observed with a constant rate given by Eq. (9) (dotted line). The inset shows the corresponding steady state concentrations of Arp (solid line) and Npf (dashed line).

density, respectively. At intermediate filament densities a smooth transition between these two limiting cases occurs.

We next couple the two models Eq. (1) and Eq. (6). For steady state growth, this can be done by either deducing the reaction order parameter  $\mu$  as a function of  $N_{fil}$  from a comparison of the branching rates in both models, or by directly inserting a filament density dependent branching rate,  $k_b = BR^{ss}(N_{fil})$ , in the branching term of an otherwise zeroth order model with  $\mu = 0$ . The second strategy turns out to be numerically more robust and will be used in the following for calculating stationary filament densities at given network growth velocity in steady state.

*Limits of autocatalytic network growth.* For a growing network at low filament density, well within the first order (autocatalytic) regime, an effective first order branching rate can be approximated by the coefficient of the linear expansion,  $k_b^{ac}$  in Eq. (8). Then  $\mu = 1$  and the contributions from capping and outgrowth of filaments integrated over all filament directions have to exactly balance filament nucleation via branching, compare Eq. (1). From this condition it is possible to derive fundamental limits of autocatalytic growth in terms of minimum and maximum capping rates  $k_c^{min}$  and  $k_c^{max}$ , corresponding to the largest and smallest possible outgrowth rate at  $v_{nw}/v_{fil} = 1$  and  $v_{nw}/v_{fil} = 0$ , respectively. By inserting the autocatalytic branching rate  $k_b^{ac}$  defined in Eq. (8)

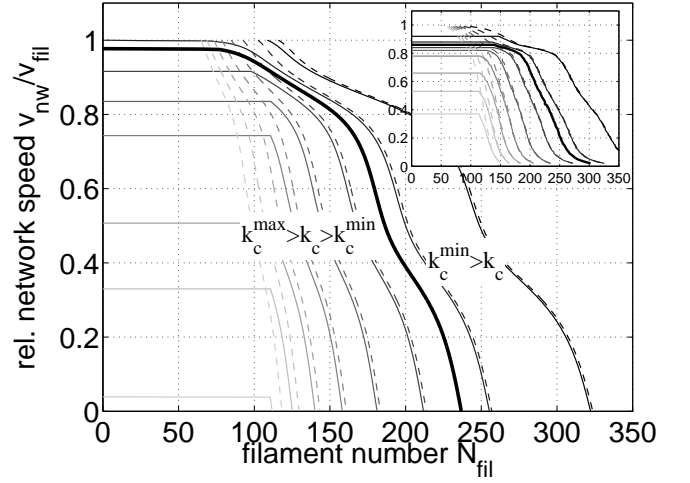


FIG. 4: Network growth velocity as a function of filament density for different capping rates obtained from the numerical solution of the full model with filament density dependent branching rates (full lines). For comparison, we show the zeroth order description with constant branching rate (dashed lines). For capping rates  $k_c^{min} < k_c < k_c^{max}$ , an autocatalytic regime with is observed at low filament density. Here the solid plateau does not agree with the dashed lines. A capping rate  $k_c = k_c^{min}$  (thick black solid line) marks the transition to a zeroth order behavior, when the solid and dashed lines start to agree. The inset shows the results from a stochastic computer simulation, which are in excellent agreement with the results from the rate equation model for the orientation distribution function.

into the first order condition, we get

$$k_c^{min} = \frac{v_{fil}}{2d_{br}} [(\cos 70^\circ - 1) + \sqrt{2 \left( \frac{k_b^{ac} d_{br}}{v_{fil}} \right)^2 + (\cos 70^\circ - 1)^2}], \quad (10)$$

and

$$k_c^{max} = \frac{k_b^{ac}}{\sqrt{2}}. \quad (11)$$

These two threshold values are also illustrated in Fig. 2b.

Fig. 4 shows the steady states of a network at various capping rate  $k_c$  by numerically solving the full model with an effective branching rate as a function of filament density (solid lines). For a capping rate  $k_c$  in between the two limits Eq. (10) and Eq. (11), an autocatalytic regime is observed at low filament density. Here, the network speed shows a plateau and thus several values for the filament density correspond to the same velocity, as it is typical for an autocatalytically growing actin network. Increasing network density above the intermediate regime, the steady state network velocity decreases like in a purely zeroth order description (dashed lines). The steady state network velocity in the autocatalytic domain drops as  $k_c$  increases, until at around  $k_c \simeq k_c^{max}$  the filament density exponentially decays to zero for all accessible network velocities. For a capping rate  $k_c \lesssim k_c^{min}$ , even the fastest



network velocity,  $v_{\text{nw}}/v_{\text{fil}} = 1$ , is not able to balance filament branching and capping via outgrowth anymore. In a purely autocatalytic description, this yields diverging filament densities. On the contrary, within our unifying framework the filament density is only able to increase until the transition to zeroth order growth takes place and thus a reasonable steady state is obtained at finite filament density. As a direct consequence, this yields  $N_{\text{fil}}$  versus  $v_{\text{nw}}$  curves (solid) with no significant difference to a purely zeroth order branching model (dashed) for such low capping rates. The inset shows the results of the stochastic network simulations, which are in excellent agreement with the numerical solution of the rate equation. This suggests that our results are very robust in regard to the details of the model implementation.

**Conclusion.** In this Letter, we have shown that conflicting predictions of two important classes of actin network growth models, namely first order branching (autocatalytic) and zeroth order branching models, can be resolved within a single theoretical framework. This unifying model yields first and zeroth order characteristics in

the limits of low and high filament density, respectively. Using this framework we have also shown that a lower threshold for the capping rate exists, below which zeroth order characteristics are predicted to dominate network growth, thus avoiding unrealistic divergences in the filament density. Although the exact activation cascade of Arp2/3 is a subject of current research, our arguments apply quite generally as long as network growth is limited by the availability of activated Arp2/3. Our results suggest to conduct experiments which systematically explore the different predicted growth regimes.

### Acknowledgments

JW was supported by the research unit for systems biology ViroQuant at Heidelberg and by the Deutsche Forschungsgemeinschaft (DFG) at Berkeley (grant no. We 5004/2-1). USS is member of the cluster of excellence CellNetworks at Heidelberg University.

- 
- [1] M. F. Carrier, ed., *Actin-based Motility* (Springer Netherlands, 2010).
  - [2] T. D. Pollard, Annual Reviews in Biophysics and Biomolecular Structure **36**, 451 (2007).
  - [3] A. Mogilner, Journal of Mathematical Biology **58**, 105 (2009).
  - [4] S. Wiesner, E. Helfer, D. Didry, G. Ducouret, F. Lafuma, M. F. Carrier, and D. Pantaloni, Journal of Cell Biology **160**, 387 (2003).
  - [5] J. L. McGrath, N. J. Eungdamrong, C. I. Fisher, F. Peng, L. Mahadevan, T. J. Mitchison, and S. C. Kuo, Current Biology **13**, 329 (2003).
  - [6] Y. Marcy, J. Prost, M. F. Carrier, and C. Sykes, Proceedings of the National Academy of Sciences of the United States of America **101**, 5992 (2004).
  - [7] S. H. Parekh, O. Chaudhuri, J. A. Theriot, and D. A. Fletcher, Nature Cell Biology **7**, 1219 (2005).
  - [8] J. Zimmermann, C. Brunner, M. Enculescu, M. Goegler, A. Ehrlicher, J. Käs, and M. Falcke, Biophysical Journal **102**, 287 (2012).
  - [9] F. Heinemann, H. Doschke, and M. Radmacher, Biophysical Journal **100**, 1420 (2011).
  - [10] M. Prass, K. Jacobson, A. Mogilner, and M. Radmacher, Journal of Cell Biology **174**, 767 (2006).
  - [11] I. V. Maly and G. G. Borisy, Proceedings of the National Academy of Sciences of the United States of America **98**, 11324 (2001).
  - [12] S. Schaub, J. J. Meister, and A. B. Verkhovsky, Journal of Cell Science **120**, 1491 (2007).
  - [13] S. A. Koestler, S. Auinger, M. Vinzenz, K. Rottner, and J. V. Small, Nature Cell Biology **10**, 306 (2008).
  - [14] J. Weichsel, E. Urban, J. V. Small, and U. S. Schwarz, Cytometry Part A **81A**, 496 (2012).
  - [15] A. E. Carlsson, Biophysical Journal **84**, 2907 (2003).
  - [16] T. E. Schaus, E. W. Taylor, and G. G. Borisy, Proceedings of the National Academy of Sciences of the United States of America **104**, 7086 (2007).
  - [17] J. Weichsel and U. S. Schwarz, Proceedings of the National Academy of Sciences of the United States of America **107**, 6304 (2010).
  - [18] S.-C. Ti, C. T. Jurgenson, B. J. Nolen, and T. D. Pollard, Proceedings of the National Academy of Sciences of the United States of America **108**, E463 (2011).
  - [19] X. P. Xu, I. Rouiller, B. D. Slaughter, C. Egile, E. Kim, J. R. Unruh, X. Fan, T. D. Pollard, R. Li, D. Hanein, et al., The EMBO Journal **31**, 236 (2012).